A 1D Ising model for ripple formation

2000 J. Phys. A: Math. Gen. 33 4955

(http://iopscience.iop.org/0305-4470/33/28/301)

J. Phys. A: Math. Gen. **33** (2000) 4955–4962. Printed in the UK PII: S0305-4470(00)09468-3

A 1D Ising model for ripple formation

Nicolas Vandewalle†‡ and Serge Galam‡

† GRASP, Institut de Physique B5, Université de Liège, B-4000 Liège, Belgium

‡ Laboratoire des Milieux Désordonnés et Hétérogènes, Tour 13, Case 86, 4 place Jussieu, 75252 Paris Cedex 05, France

Received 10 November 1999, in final form 8 May 2000

Abstract. A 1D Ising model is shown to reproduce qualitatively the dynamics of ripple formation. The saltation effect is imposed using a Kawasaki dynamics and a pair interaction over some distance ℓ. Within this model, the ripple state turns out to be metastable, in agreement with cellular automata simulations as well as recent underwater experiments. A dynamical phase diagram is obtained. A mean-field solution of the problem is given in terms of the ripple size. A mapping is then performed onto a 2D $\ell \times \infty$ static problem.

1. Introduction

Ising spin models have been used to describe a wide range of physical and non-physical problems [1, 3]. Amongst others, they have proven useful in understanding some aspects of granular media, in particular, compaction dynamics under tapping [1, 2].

Here we present a simple 1D Ising model to describe qualitative features of ripple formation. Previous experimental and theoretical work has underlined the primary role played by saltation in the emergence of sand ripples and dunes [4–7]. Saltation means grain ejection and aeolian transport over long distances. The hopping and rolling of grains have generally led to travelling ripple structures, which in turn merge and grow.

In the following, an Ising spin description of the dynamics of ripple formation is presented. A 1D Hamiltonian is suggested. It is studied numerically with a Kawasaki dynamics. A mean-field treatment is also performed. A dynamical phase diagram is obtained. Results are discussed and compared with recent cellular automaton results [8] and with recent underwater experiments [4].

2. The model

A natural way to map a 1D granular landscape into a spin model is to consider a 1D Ising model $\{\sigma_i = \pm 1\}$. Let the wind blow from left to right. At each site i, $\sigma_i = +1$ if the local slope is positive (exposed to the wind). It is $\sigma_i = -1$ if the local slope is negative (screened by the ripple crest and unaffected by the wind). Successive slopes are then associated with the succession of spin domains. Spin domains represent the ripple sides. A sketch of such a mapping is shown in figure 1.

In figure 1, a grain is first shifted over a distance $\ell = 7$ by saltation. An avalanche then occurs to relaxe the surface. From the magnetic viewpoint, both extraction and relaxation of one grain produce two pairs of spin flips, meaning that the whole dynamics proceeds by spin pairs.

0305-4470/00/284955+08$30.00

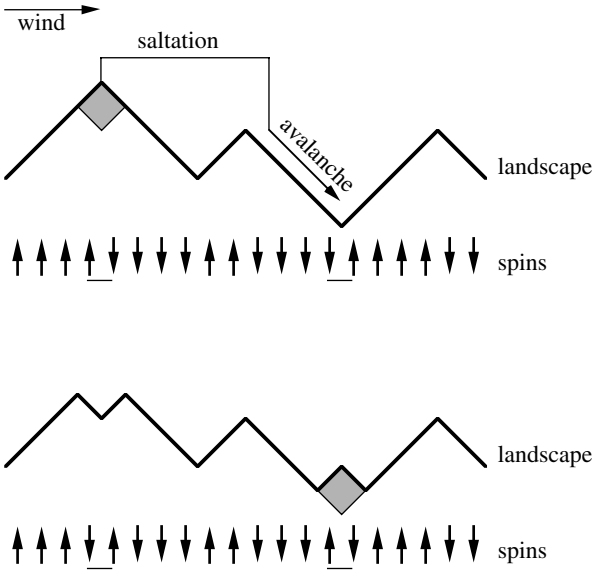

Figure 1. (Top): sketch of the rule. A grain at position i is unstable and is carried by the wind to position $i+\ell$ where an avalanche relaxes the surface. Spin signs indicate the slope of the landscape. (Bottom): after the saltation–avalanche event, the magnetization remains unchanged.

Moreover, it proves that the dynamics does not modify the total magnetization $m = \sum_i \sigma_i$. To embody these physical effects characterizing the saltation–avalanche mechanism, we consider the so-called Kawasaki dynamics [9]. Having a 1D Ising system the equilibrium total magnetization is zero. In addition, it will stays zero since the Kawasaki dynamics preserves the total magnetization.

Avalanches which relax the granular surface can be viewed as small thermal fluctuations along the ripple sides. In our spin mapping such a scheme corresponds to a ferromagnetic nearest-neighbour coupling J_{nn} divided by $k_{\mathrm{B}}T$, where T is the temperature and k_{B} is Boltzmann's constant. Moreover, saltation occurs only on the faces exposed to the wind and leads to a perturbation at the position $i+\ell$, where ℓ is the distance over which the sand is transported by saltation. As for avalanches, we mimic this effect by a ferromagnetic coupling J_{s} which connects a site i to a site $i+\ell$, divided by $k_{\mathrm{B}}T$.

On this basis we consider the following dimensionless Hamiltonian:

$$E = -K_{\mathrm{nn}} \sum_{i=-\infty}^{+\infty} \sigma_i \sigma_{i+1} - K_{\mathrm{s}} \sum_{i=-\infty}^{+\infty} \sigma_i \sigma_{i+\ell} \delta_{\sigma_i,+1} \tag{1}$$

where $\delta_{x,y}$ is the Kronecker function, $K_{\mathrm{nn}} \equiv \frac{J_{\mathrm{nn}}}{k_{\mathrm{B}}T}$ and $K_{\mathrm{s}} \equiv \frac{J_{\mathrm{s}}}{k_{\mathrm{B}}T}$. The Kronecker delta function in the second term assumes that only faces exposed to the wind (spins +1 for a wind blowing from left to right) play a role for saltation. These assumptions seem reasonable and not of any drastic consequence at our present level of investigation.

3. Numerical simulations

Numerical simulations have been performed on a 1D system with periodic boundary conditions, i.e., a loop. The initial spin loop configuration is random, with $m = 0$. Thereafter, one positive spin and one negative spin are randomly selected at each time step. The energy variation ΔE

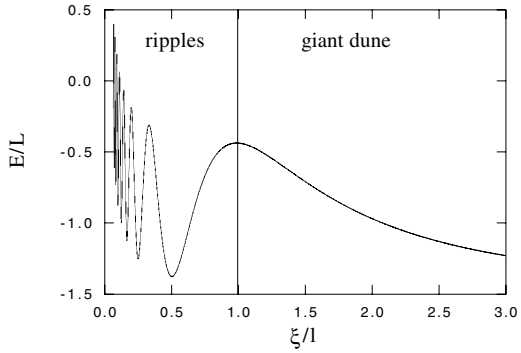

Figure 2. Typical space–time patterns in which domain walls are drawn: $L = 144$ and $\ell = 21$. Three different sets of parameter values are shown: (*a*) $K_{\rm nn} = 0.5$ and $K_{\rm s} = 0.5$, (*b*) $K_{\rm nn} = 2.0$ and $K_{\rm s} = 2.5$, and (*c*) $K_{\rm nn} = 2.5$ and $K_{\rm s} = 0.5$.

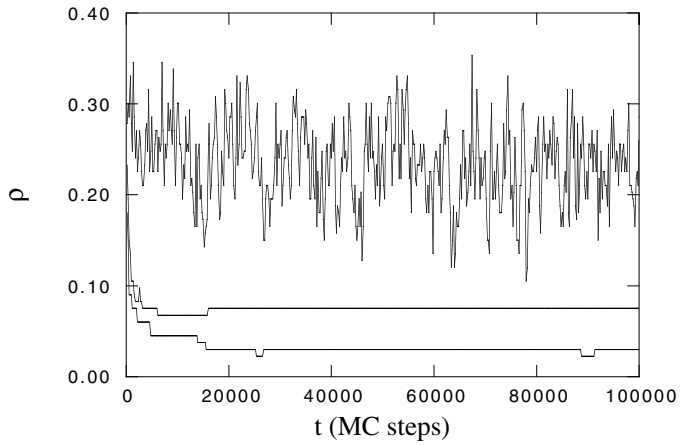

Figure 3. The density of domain walls ρ as a function of time. Three different sets of parameter values are shown, from top to bottom: $K_{\rm nn} = 0.5$ and $K_{\rm s} = 0.5$, $K_{\rm nn} = 2.0$ and $K_{\rm s} = 2.5$, and $K_{\rm nn} = 2.5$ and $K_{\rm s} = 0.5$.

due to the flipping of both selected spins is calculated. Periodic boundary conditions are used in the energy calculation. The selected spins are then flipped with some probability $p = \frac{\exp \Delta E}{1+\exp \Delta E}$ as in classical Monte Carlo methods [9]. The fact that two opposite spins are chosen at each time step preserves the $m = 0$ value of the order parameter during the whole simulation, i.e., a Kawasaki dynamics.

Since the magnetization m is zero and constant, a dynamical 'order parameter' can be defined with the domain wall density ρ, i.e. the density of nearest-neighbour antagonist pairs of spins. One should note that

$$\rho = \frac{\xi}{L} \tag{2}$$

where ξ is the mean size of the spin domains. Loop lengths up to $L = 10\,000$ spins have been used. Our numerical results have been checked against variation in the parameters ($K_{\rm nn}$, $K_{\rm s}$ and ℓ). Finite-size effects, as well as the spin pattern time evolution, have also been analysed. It is worth noting that ℓ and L have always been chosen to be incommensurate in order to avoid

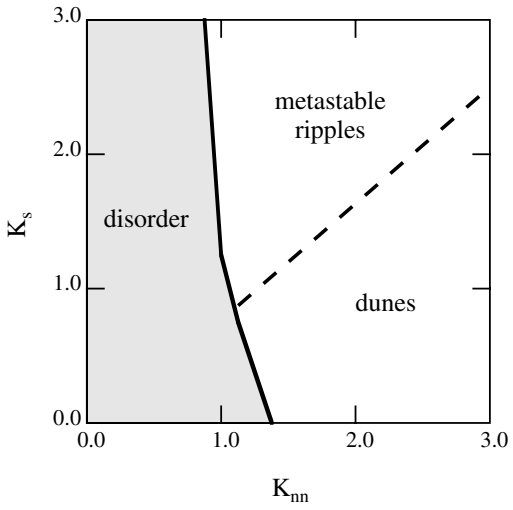

Figure 4. The dynamical phase diagram (K_s versus K_{nn}) of the model. The disorder phase is represented in grey in the diagram. The order phase is represented in white. Ripples and dunes are also distinguished.

any artefact due to the periodic boundary conditions.

Figure 2 presents typical space–time patterns in which domain walls are drawn for characteristic lengths $L = 144$ and $\ell = 21$. Three different sets of parameter values K_{nn} and K_s are shown. Depending on the parameter values three different regimes are obtained. Either disorder (figure 2(a)), or order with domains of roughly the size $\ell/2$ (figure 2(b)), or also order with larger domains (figure 2(c)). Domains having a size of the order $\ell/2$ are thereby called 'ripples'. In parallel, much larger domains are called 'dunes' in reference to simulations in [8].

Figure 3 contains the domain wall density ρ as a function of time for the three regimes of figure 2. The following is observed: (i) an erratic signal for the disordered regime presenting huge fluctuations of ρ, (ii) an apparently stable density $\rho \approx \ell/2$ after a short transient regime, and (iii) a low density regime ($\rho \approx 0$) decorated with small fluctuations after some transient regime.

Figure 4 is the associated resulting dynamical phase diagram as a function of (K_{nn}, K_s) obtained numerically for $\ell > 1$. Three different dynamical regimes are thus found. A region of the disorder regime is represented in grey in the phase diagram. The boundary with the order regime is found to be stable whatever the values of $\ell > 1$ and L. Curves $\rho(K_{nn})$ are shown in figure 5 for different values of K_s where one can clearly see a crossover around $K_{nn} \approx 1$. At this point, the domain size is equivalent to $\ell/2$. Moreover, this boundary is stable in time. This result could be astonishing since finite-size effects are expected. One should recall that $m = 0$ corresponds to the equilibrium state of a 1D Ising model and thus fluctuations and the domain wall evolution take place in the equilibrium state. Those are mainly driven by the Ising interaction K_{nn}.

For the order regime (white region in figure 4), two distinct regions coexist: ripples (for $K_s \gg K_{nn}$) and dunes (for $K_{nn} \gg K_s$). The dashed line in figure 4 represents the boundary between these regimes. However, this boundary moves slightly when the system size L or the saltation length ℓ is changed. In fact, the ripple state is metastable. After very long times, ripples can suddenly merge into dunes (as seen by geologists). The larger K_s is, the more stable ripples are.

Different initial correlations have been examined. Starting from a perfect antiferromagnetic situation, the system reaches the same regimes as described above. The

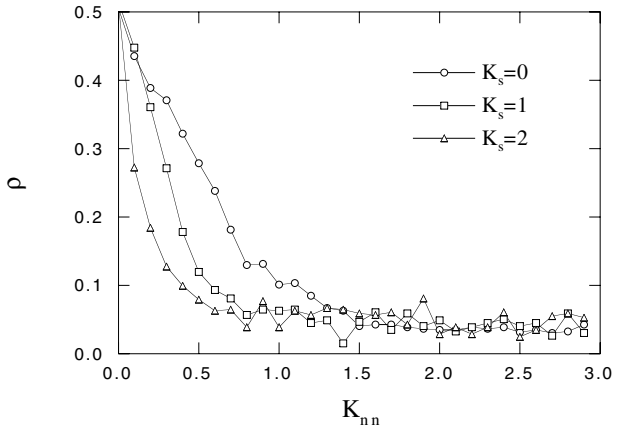

Figure 5. The density of domain walls ρ as a function of the Ising interaction $K_{\rm nn}$. Three different values of $K_{\rm s}$ are shown. The crossover separating disorder and order regimes is emphasized.

dynamics is similar to what we have observed for the random initial situation. However, if one starts with a system containing only two large domains, i.e. a single giant dune, the system never produces ripples but remains unchanged in the order region of the dynamical phase diagram. In the disorder regime (in grey in figure 4), the initial giant dune is, however, destroyed.

Finally, one should note the case $\ell = 1$ is quite particular. In that case, spin domains are produced even when $K_{\rm nn} = 0$ for which a disorder regime is expected. As soon as $\ell > 1$, the results summarized in figure 4 are recovered.

4. Mean-field treatment

Even though the Hamiltonian (1) is rather simple, it does not allow for an easy exact solution. For instance, the classical method of the transfer matrix [10] leads to searching for $2^{\ell+1} \times 2^{\ell+1}$ matrices. In order to solve this problem, we have considered as a first approximation that the mean domain size ξ is the relevant parameter. Fluctuations in ξ are neglected.

Assuming an order with domains of size ξ, the first product $\sigma_i\sigma_{i+1}$ of equation (1) gives $\frac{\xi-2}{\xi}$ due to the presence of domain walls which are energetically unfavourable. The second product $\sigma_i\sigma_{i+\ell}$ of equation (1) gives a periodically oscillating function of period 2ξ. Thus, the energy per lattice site E/L can be written as

$$\frac{E}{L} \approx -K_{\rm nn}\left(\frac{\xi-2}{\xi}\right) - \frac{K_{\rm s}}{2}\cos\left(\frac{\pi\ell}{\xi}\right) \tag{3}$$

which is drawn in figure 6 as a function of ξ and for arbitrary values of the coupling energies $K_{\rm nn}$ and $K_{\rm s}$. Several minima are observed. The selection of various lengths $\ell/2$, $\ell/3$, $\ell/4$, ... is thus expected from the above shape of $E(\xi)$. The more stable local minima is for $\ell/2$, i.e., it corresponds to ripples of size ℓ.

For $\xi > \ell/2$, a large potential barrier separates the ripple state from the 'giant dune' state. The asymmetry of this barrier implies the irreversibility of the 'ripple $\rightarrow$ dune' process. The ripple metastability is thus also obtained from a mean-field treatment, in agreement with the above numerical results.

Nevertheless, the mean-field solution does not predict any disordered dynamical regime. Indeed, fluctuations of ξ are neglected. Fluctuations destroy the order when $K_{\rm s}$ is small.

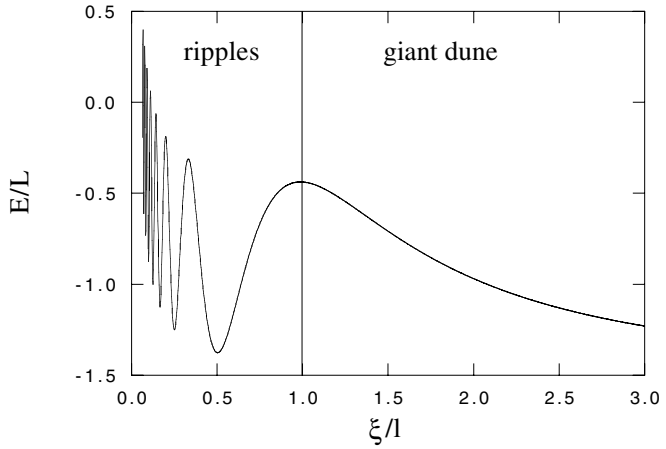

Figure 6. Typical shape of the energy per lattice site E/L as a function of the normalized domain size ξ/ℓ.

5. Mapping onto a 2D $\ell \times \infty$ static problem

Although ripple formation is a *dynamical* phenomenon, our study is generated via Monte Carlo (equilibrium-like) simulations. The dynamical aspect survives only because the relaxation towards equilibrium is slow and hampered by metastability.

Another remark concerns equation (1). Upon setting $\delta_{\sigma_i,+1} = \frac{1}{2}(1 - \sigma_i)$ in equation (1), multiplying out the σs, and using the fact that $m = \sum_i \sigma_i$ one finds

$$E = -K_{\rm nn} \sum_i \sigma_i \sigma_{i+1} - K_{\rm s} \sum_i \sigma_i \sigma_{i+\ell} + \tfrac{1}{2} K_{\rm s} m \tag{4}$$

in which the last term is an irrelevant constant that is set equal to zero later. Now, replace each site index i by two integer coordinates j and k uniquely defined by the conditions

$$i \equiv j\ell + k \qquad \text{with} \quad k \in \{0, 1, \ldots, \ell - 1\} \tag{5}$$

and write $\sigma_i = \sigma_{j,k}$. In terms of these new variables the Hamiltonian equation (4) takes the form

$$E = -K_{\rm nn} \sum_{j=-\infty}^{\infty} \sum_{k=0}^{\ell-1} \sigma_{j,k} \sigma_{j,k+1} - K_{\rm s} \sum_{j=-\infty}^{\infty} \sum_{k=0}^{\ell-1} \sigma_{j,k} \sigma_{j+1,k} \tag{6}$$

provided we interpret (j, k) as a site on an $\ell \times \infty$ cylindrical lattice with screw boundary conditions (CL/SBC) around the cylinder. Hence E of equation (6) describes Onsager's anisotropic nearest-neighbour Ising model on a CL/SBC, but with the additional constraint $m = 0$.

This sheds an interesting light on the simulation results. The relevant facts are:

(a) The constraint $m = 0$ and the SBC are irrelevant for the thermodynamics of this model, which is therefore the same as that of the Onsager model without constraint and in zero magnetic field.

(b) The $\ell \times \infty$ lattice has no phase transition. But in the limit $\ell \to \infty$ this model does have the ferromagnetic Onsager phase transition. Of course, for ℓ sufficiently large, simulations will show an order/disorder transition-like behaviour.

(c) The ground state $\mathcal{G}_0$, due to the condition $m = 0$, necessarily has an interface. If the j direction (the one parallel to the cylinder axis) is infinite, $\mathcal{G}_0$ is a cylinder which is

positively magnetized for $j > 0$ and negatively magnetized for $j \leqslant 0$. If the j direction is finite (let us say $-J < j \leqslant J$ for some J), then $\mathcal{G}_0$ is still a low-lying state of energy $E(\mathcal{G}_0) \sim -\ell K_s$, but another low-lying state appears, namely the state $\mathcal{G}_1$ which has positive magnetization for $\ell/2 \leqslant k \leqslant \ell - 1$ and negative magnetization for $0 \leqslant k < \ell/2$ (ℓ supposed even for convenience). Its energy is $E(\mathcal{G}_1) \sim -2JK_{nn}$. Both states are local energy minima in configuration space (because in both the interface length is at a local minimum) and, with the Kawasaki dynamics of this paper, the higher one of the two states is metastable with respect to the lower one. It is evident that $\mathcal{G}_0$ corresponds to the 'dune' and $\mathcal{G}_1$ to the 'rippled state'.

6. Connection to recent underwater experiments

The physics underlying both ripple and dune formation is far from being understood, making any analytic result valuable. Indeed, it has been believed that dune dynamics are of a different nature to ripple dynamics. Moreover, the question of a ripple growing to eventually produce a dune is still open.

Bagnold [11] distinguished ripples and ridges. Periodicity of the former ones was time independent while periodicity of the latter ones was growing with time. The present work suggests in a simple way that both patterns are two aspects of the same phenomenon since the ripple state seems to be metastable.

Recent experiments of underwater sand [4, 12] have exhibited the formation of ripples. There, sudden merging of ripples does also occur in qualitative agreement with our results (see the upper part of the dynamical phase diagram of figure 4). Moreover, these authors have found that a 'transition' takes place between a flat landscape regime and ripple formation at a critical value of the Reynolds number, Re. This feature is to be put in parallel to the transition that we have obtained (see figure 4) between a disordered regime and a ripple dynamical regime. Indeed, the saltation length ℓ could be directly connected to the physical parameter Re.

7. Comparison with a cellular automaton

In addition, a recent cellular automaton model [8] did produce a dynamical ripple state which eventually stabilizes into a giant dune. This model considers a granular landscape for which surface local fluctuations are dissipated through both saltation and avalanches [13]. Saltation is restricted to grains exposed to the wind while avalanches occurs everywhere.

The associated dynamics is rather complex. First, ripples appear. Secondly, they coalesce very slowly into 'giant dunes'. The main features of ripple and dune formation are recovered within the present spin framework, except for the disordered regime which is absent in [8].

Even though the cellular automaton model, as well as the actual spin-like model, are far from real desert dunes and ripples, they seems to reproduce some analogous features.

8. Conclusion

In summary, we have proposed a 1D Ising model for ripple formation. The spin model has been studied numerically. In addition, a mean-field solution for the ripple size was also obtained. Moreover, the ripple state has been found to be metastable, a result which is in full agreement with very recent experiments under water as well as previous landscape simulations.

Nature is obviously much more complex than a 1D spin model. However, our very simple description reproduces some basic features of dune formation, as seen above. Moreover, the model could be extended to include, for instance, a distribution of saltation lengths or even

different grain types. This is left for future work. We do hope our results will stimulate additional experimental work, in particular to check our dynamical phase diagram.

Acknowledgments

NV thanks the FNRS (Brussels, Belgium). He also thanks the LMDH for its hospitality during the progress of this work. We would like to thank Dr H J Hilhorst for a very stimulating comment.

References

[1] Nicodemi M, Coniglio A and Herrmann H 1997 *Phys. Rev.* E **55** 3962
[2] Piccioni M, Nicodemi M and Galam S 1999 *Phys. Rev.* E **59** 3858
[3] Galam S 1997 *Physica* A **238** 66
[4] Betat A, Frette V and Rehberg I 1999 *Phys. Rev. Lett.* **83** 88
[5] Anderson R S 1990 *Earth Sci. Rev.* **29** 77
[6] Terzidis O, Claudin Ph and Bouchaud J P 1998 *Eur. Phys. J.* B **5** 245
[7] Csahok Z, Misbah C and Valance A 1999 *Physica* D **128** 87
[8] Vandewalle N and Galam S 2000 *Int. J. Mod. Phys.* C **10** at press
[9] Binder K (ed) 1979 Monte Carlo methods *Topics in Current Physics* (Berlin: Springer)
[10] Stanley H E 1971 *Phase Transitions and Critical Phenomena* (Oxford: Oxford University Press)
[11] Bagnold R A 1941 *The Physics of Blown Sand and Desert Dunes* (London: Chapman and Hall)
[12] Stegner A and Wesfreid J E 1999 *Phys. Rev.* E **60** R3487
[13] Bak P, Tang C and Wiesenfeld K 1987 *Phys. Rev. Lett.* **59** 381